Egyptian Geophysical Society
EGS Journal, Vol. 15, No. 1, 89-95 (2017)

POST-STACK SEISMIC INVERSION FOR LAND SEISMIC DATA NORTHERN WESTERN DESERT, EGYPT

A. El-Werr[1], M.M.F. Shokry[1], A. Shebl[1], and A. Elmidany[2]

1- Geophysics Department, Faculty of Science, Ain Shams University
2- Senior Field Geophysicist at Arabian Gas Seismic Company, KSA

الانقلاب السيزمى بعد التكديس للمعطيات الأرضية

بشمال الصحراء الغربية

الخلاصـــة: تعد رزمة انعكاس السيزمية والإجراء لاستخراج النموذج الأساسي مـــن الخصـــائص الفيزيائيـــة للصخوروالســـوائل. فهـــو يســـتخدم لتقديرالخصائص الفيزيائية للصخورمن خلال الجمع بين البيانات السيزمية وتسجيلات الآبار. وقد ثبت بعد رزمة انعكاس الزلزالي أن تكـــون نظريـــة مفيدة جدا في الكشف عن تواجد النفط والغاز وتعريف الصخرية في منطقة الدراسة. كان أقل مقاومة الشذوذ الصوتية واضح جدا تؤكد تواجـــد الـــنفط والغازفي منطقة الفائدة في منطقة الدراسة لدينا والتي هي طبقة الخزان علم البويب ٣ج. أيضا،كان هذا النهج مفيدا جدا في الكشف عن أعلى الشـــذوذ مقاومة الصوتية على مستوى طبقة العلمين تشكيل نظرالوجود من الدول وميتوالصخرالزيتي كما الصخور الخام.

ABSTRACT: *Post stack seismic inversion is the procedure for extracting underlying model of the physical characteristics of rocks and fluids. It is used to estimate the physical properties of the rocks by combining seismic and well logs data. Post stack seismic inversion has proven to be very useful theory in the detection of the hydrocarbon occurrences and lithological definition in the area of study. Lower acoustic impedance anomaly was very clear confirming the hydrocarbon occurrences at the zone of interest in our study area which is Alam El Bueib 3G reservoir member. Also, this approach was very helpful in the detection of higher acoustic impedance anomaly at the level of Alamein Formation due to the presence of dolomite and shale as seal rocks.*

INTRODUCTION

North Matruh study area lies in the northern part of the Western Desert, Egypt. It is found between latitudes 31° 3' 2.5"&30° 52' 48" N and longitudes 26° 56' 38.4"&27° 13' 48" E as shown in the study area location map (Figure 1).

The interest in seismic inversion techniques has been growing steadily over the last twenty years, Post-seismic inversion is the procedure for extracting underlying models of the physical characteristics of rocks and fluids. Itis used to estimate the physical properties of the rocks by combining seismic and well log data, i.e. from the continuous data set. In many cases, the physical parameters of interest are the impedance, velocity and density. Usually, the inversion procedure depends on some form of forward modeling generating the earth's response to a set of model parameters by using mathematical relationships. The post-stack AI inversion method started in the early 80□s when algorithms of wavelet amplitude and phase spectra extraction became available (Lindseth, 1979). Inversion results showed high resolution, enhanced the interpretation, and reduced drilling risk (Pendrel, 2006).

Inversion replaces the seismic signature by a blocky or layered response, corresponding to acoustic and/or elastic impedance (AI or EI) earth model. The seismic inversion transform the seismic contrast model into layer cake model, it facilitates the interpretation of meaningful geological and petrophysical boundaries in the subsurface. It results in optimized volumetric, improved ranking of prospects, better delineation of drainage areas and identification of 'sweet spots' in field development studies.

The main benefits of seismic inversion according to Curia, 2009 are:

- More geoscientists understand the concept of impedance and geology than the seismic trace. Thus, working in the impedance domain is a great mechanism for integrating with the various disciplines in a multidisciplinary asset team.
- Removes the effects of the wavelet within the seismic bandwidth.
- Forces well ties to be made and understood.
- Reservoir properties are separated from the overburden.
- May provide quantitative predictions on the reservoir properties.
- Stratigraphic interpretation may be improved.
- Interpreting in the impedance domain is frequently easier than in the seismic domain.
- Possibility of extending beyond the seismic bandwidth.

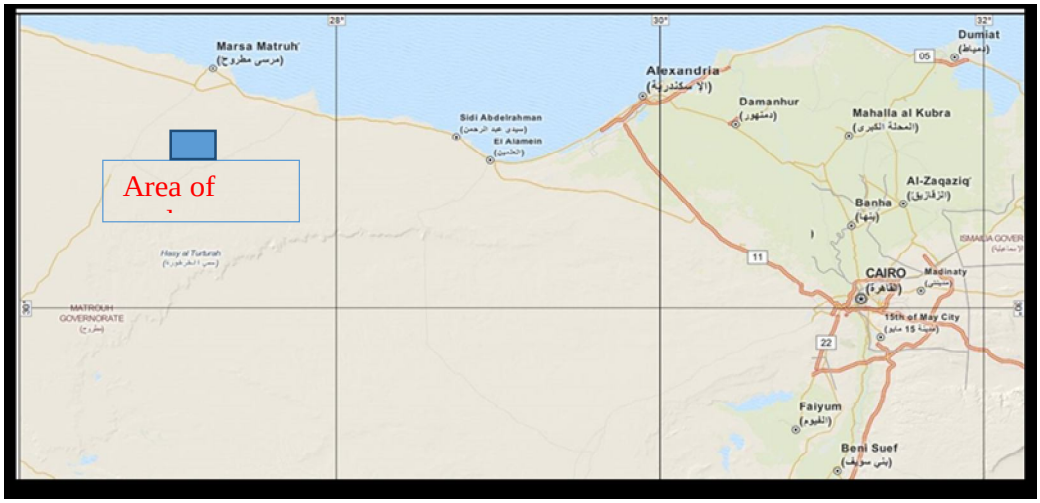

Figure 1: Location map of the study area.

Figure 2 illustrates the general principle of the post-stack AI inversion. Well log data provides the missing frequencies (Lows and highs frequencies ranges). Non-uniqueness of the solution is another problem, and seismic data can lead to multiple possible geologic models which are consistent with the observations. In addition, in the inversion method itself, multiple reflections, transmission loss, geometric spreading and frequency-dependent absorption are ignored. The common way to reduce these uncertainties is to use additional information (mostly coming from well logs) which contains low and high frequencies and constrains the deviations of the solution from the initial-guess model. The final result therefore relies on the seismic data as well as on this additional information, and also on the details of the inversion methods themselves.

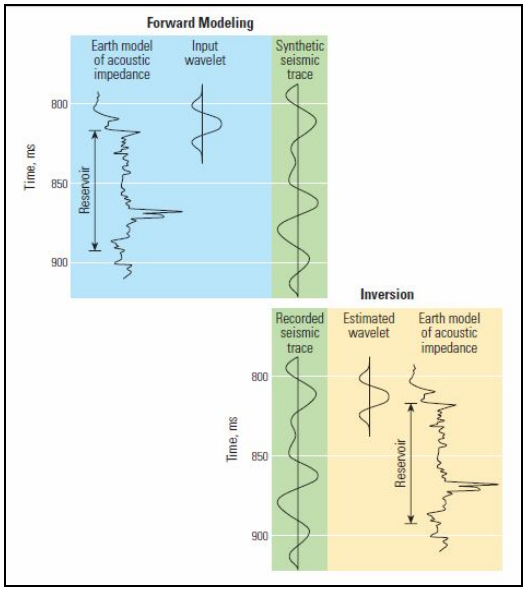

Figure 2: Illustrates the general principle of the post-stack AI inversion.

Post-Stack Simultaneous SeismicInversion

Inversion is the act of determining features of something by observing its effects, on seismic data in this case. In practice, we use inversion techniques to determine the seismic impedance (velocity times density) Hampson Russell, 2004,by removing the wavelet (treated as a bandpass filter) that comes from the acquisition and procession steps. Well control scales this wavelet and restores the low frequency component.

The process is:

1. Determine a layer model of reflection coefficients with a source wavelet and seismic data.
2. Calculate the resulting impedances.
3. Ensure that the model meets the constraints.

In other words, it can be thought of as:

Lm + n = s,

Where L is the linear operator that links the model to actual seismic (i.e., it turns the model into a synthetic volume), n is noise and s is the actual seismic data (the actual recorded traces). In some publications, "d" is used for data instead of "s"

$$s_i = \sum_j^N r_j W_{i-j+1} + n_i$$

where: rj = the zero-offset reflectivity of the earth

Wi= the seismic wavelet, assumed to be constant

ni = additive measurement noise

Results of Post-Stack Inversion

1. Wavelet Extraction:

All modern seismic inversion methods require seismic data and a wavelet estimated from the data. Typically, a reflection coefficient series from a well

within the boundaries of the seismic survey is used to estimate the wavelet phase and frequency. Accurate wavelet estimation is critical to the success of any seismic inversion. The inferred shape of the seismic wavelet may strongly influence the seismic inversion results and, thus, subsequent assessments of the reservoir quality.

Wavelet amplitude and phase spectra are estimated statistically from either the seismic data alone or from a combination of seismic data and well control using wells with available sonic and density curves. After the seismic wavelet is estimated, it is used to estimate seismic reflection coefficients in the seismic inversion.

When the estimated (constant) phase of the statistical wavelet is consistent with the final result, the wavelet estimation converges more quickly than when starting with a zero phase assumption. Minor edits and "stretch and squeeze" may be applied to the well to better align the events. Accurate wavelet estimation requires the accurate tie of the impedance log to the seismic. Errors in well tie can result in phase or frequency artifacts in the wavelet estimation. Once the wavelet is identified Figure 3, seismic inversion computes a synthetic log for every seismic trace. To ensure quality, the inversion result is convolved with the wavelet to produce synthetic seismic traces which are compared to the original seismic.

Wavelet extraction is the first step of the inversion. The next parameters have been used for creating synthetic seismogram and extracting the wavelet:

Start time	*1450ms*
End time	*2000ms*
CMP range	*426 - 486*
Taper	*100ms*
Phase	*134 deg*

The parameters used for wavelet extraction are: the time range of 1450-2000 ms was suitable for our target, which is between 1600 and 2000 ms. once the wavelet was extracted, well-log correlation was performed for each well. The correlation was applied as follows:

A synthetic trace was generated and compared to the real seismic trace nearest to the well location; Time shifting was applied to align the seismic and well-log events; Correlation coefficient was measured between the seismic and adjusted well-log synthetic traces Corresponding seismic data. The correlations were good for all wells (above 74%). As an example, Figure 4 shows the correlation of the reflection synthetics with well logs at Well Jade#4.

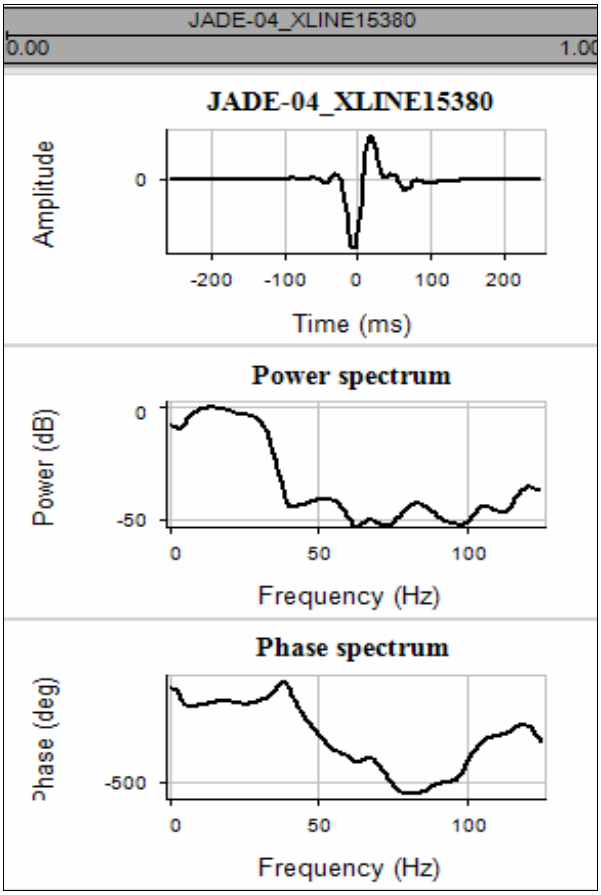

Figure 3: Showing the extracted wavelet and spectral analysis.

2. Initial Low Frequency Model Building

Data required for LFM

1- Extracted wavelet as shown above.

2- Log-to-seismic correlation and horizon picking.

Determination of the starting model was the next step of the inversion. This model was built by generating the AI from the well location into the in-lines shown in Figure5, two interpreted seismic horizons were introduced to guide the structural information.

A 10-Hz low-pass filter was applied to the model for two reasons: First, the low-frequency impedance trend was required in order to recover the low frequencies missing from the stacked seismic data. In addition, the impedances above ~10-Hz frequencies should be only obtained from seismic data, and therefore this frequency band should be removed from the well-log data while building the starting model. Going through the steps we got intermediate output results for relative acoustic impedance and low frequency model as shown in Figures 6 and 7 to get the main output of the process which is acoustic impedance output result as shown in Figure 8.

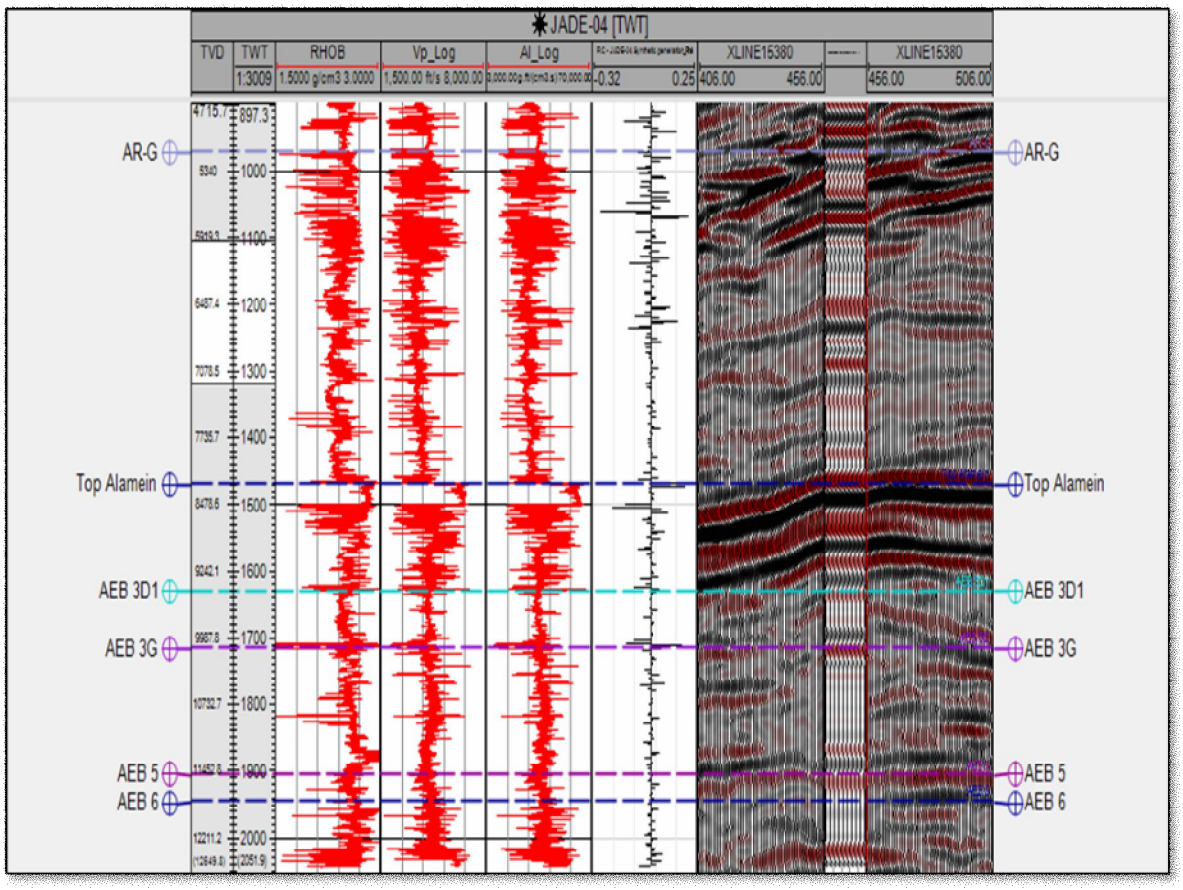

Figure 4: Correlation at well Jade#4 by using the deterministic wavelet. The curves, left to right, show: well density log, P-wave velocity log, AI Log and the Synthetic trace from the well. The seismic trace, for easy comparison each trace repeated several times. The Correlation level is 74%.

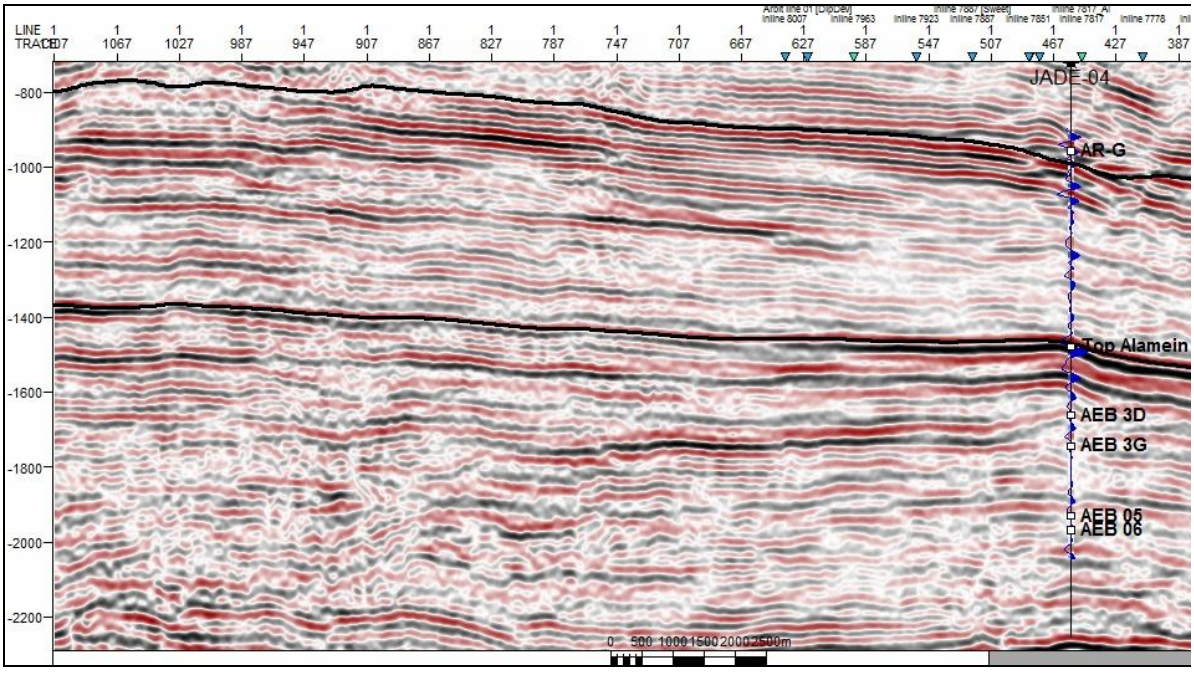

Figure 5: Seismic section for cross line15380.

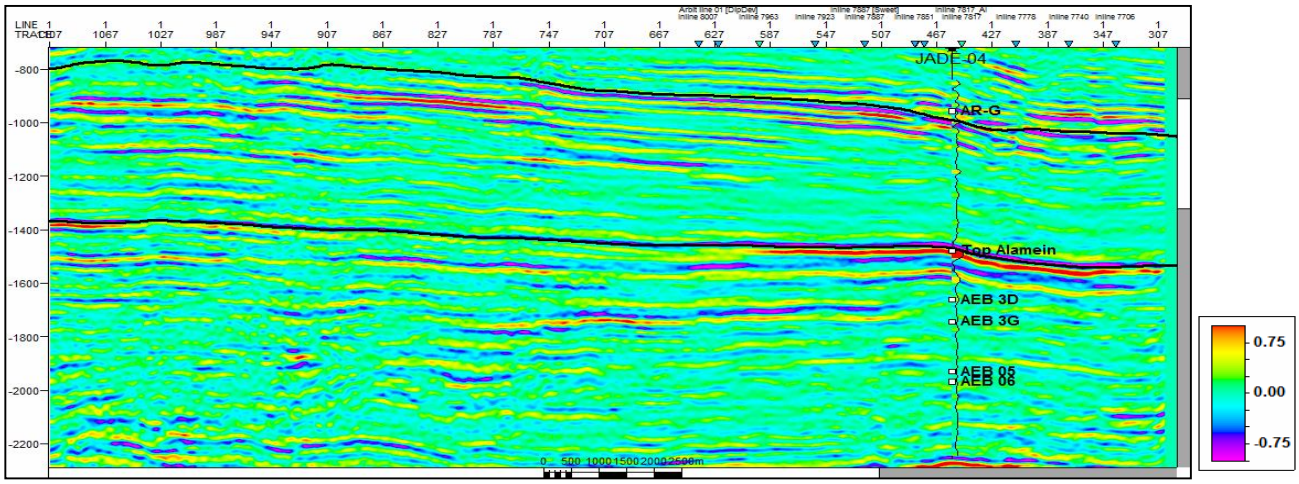

Figure 6: Relative acoustic Impedance Section for cross line 15380

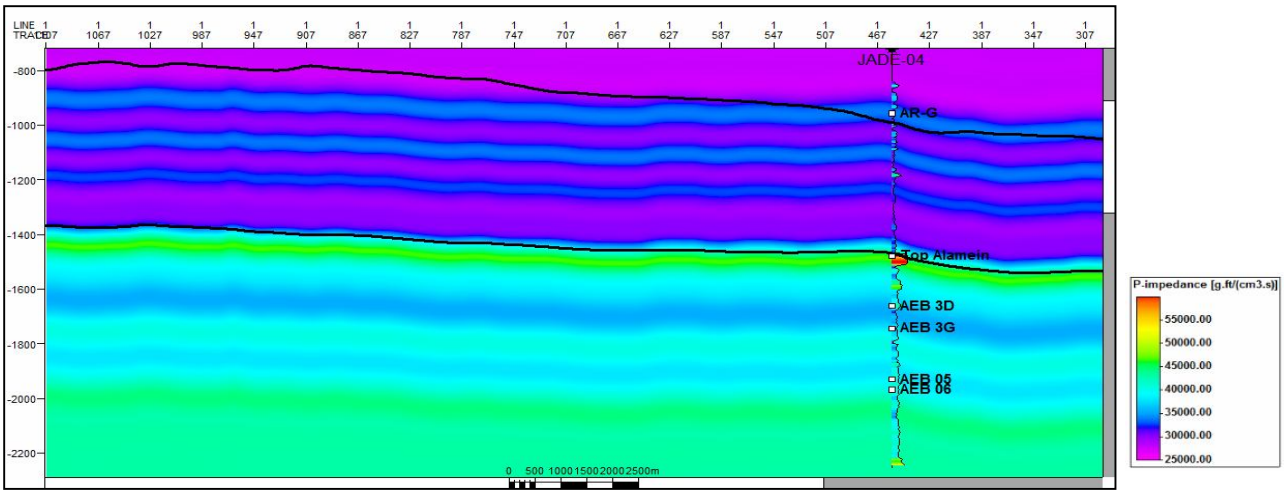

Figure 7: Low Frequency Model for cross line 15380.

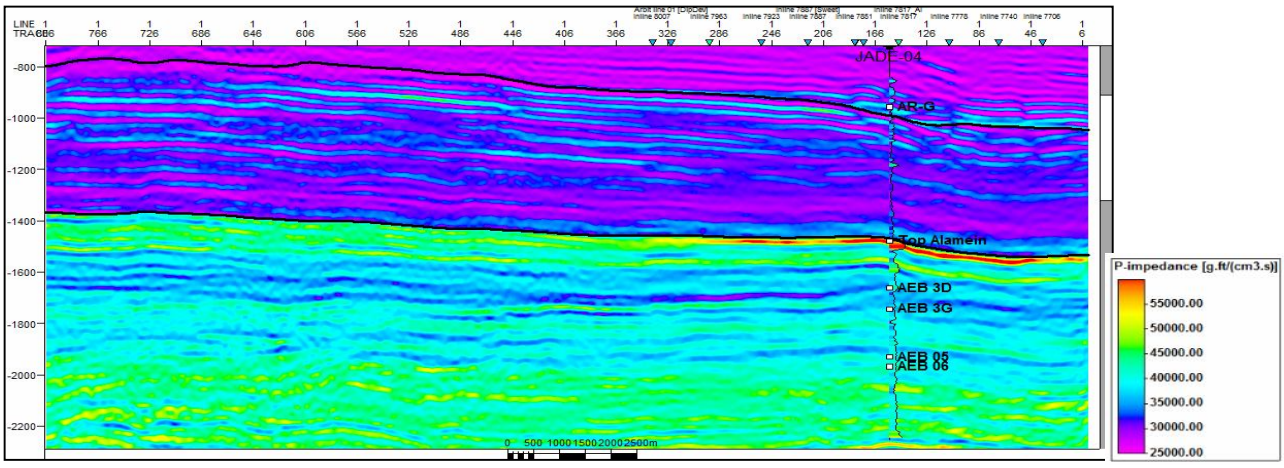

Figure 8: Acoustic Impedance Section for cross line 15380.

From the mentioned Figures above we can deduce the following features:

Lower acoustic impedance anomaly was a good indicator for the presence of hydrocarbon at the zone of interest in our study area which is Alam El Bueib 3G reservoir member. Also, the detection of higher acoustic impedance anomaly at the level of Alamein Formation due to the presence of dolomite and shale seal rocks

3. Model Based Inversion

Model based inversion was the first inversion procedure applied to the dataset. The following parameters have been used:Inversion time interval: 500-2800 ms; High cut frequency: 10Hz

The inversion result at the well location was compared to the original log at well Jade04 as shown in Figure 8. In general, the inverted AIwas comparable to the well-log impedance. Synthetic traces generated fromthe resulting AI were correlated with the seismic traces for all wells. Following the same steps applied above we got intermediate output results for relative acoustic impedance and low frequency model as shown in Figures 10 and 11 to get the main output of the process which is acoustic impedance output result as shown in Figure 12.

A cross section of the inversion result is given in Figure 12. Note that low impedances near 1750ms level are clearly visible in this Figure which is the level of reservoir.

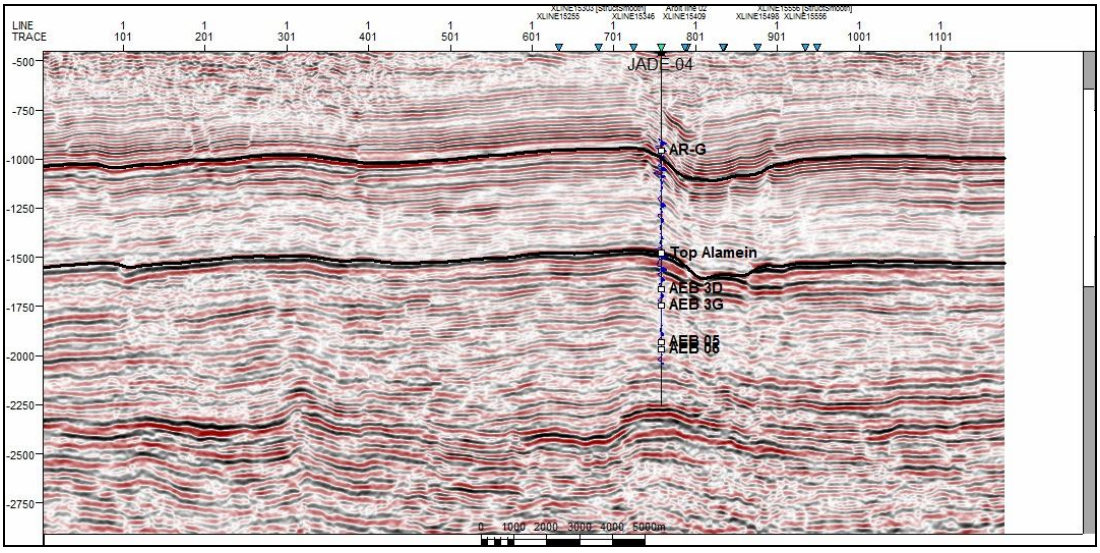

Figure 9: Seismic Section for Inline 7817.

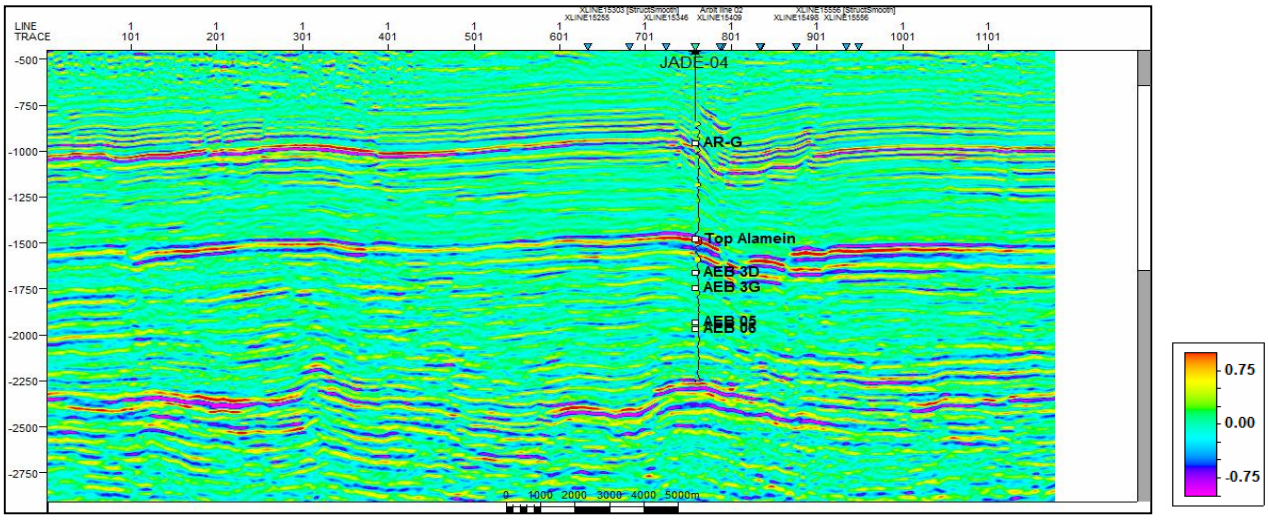

Figure 10: Relative acoustic Impedance Section for Inline 7817.

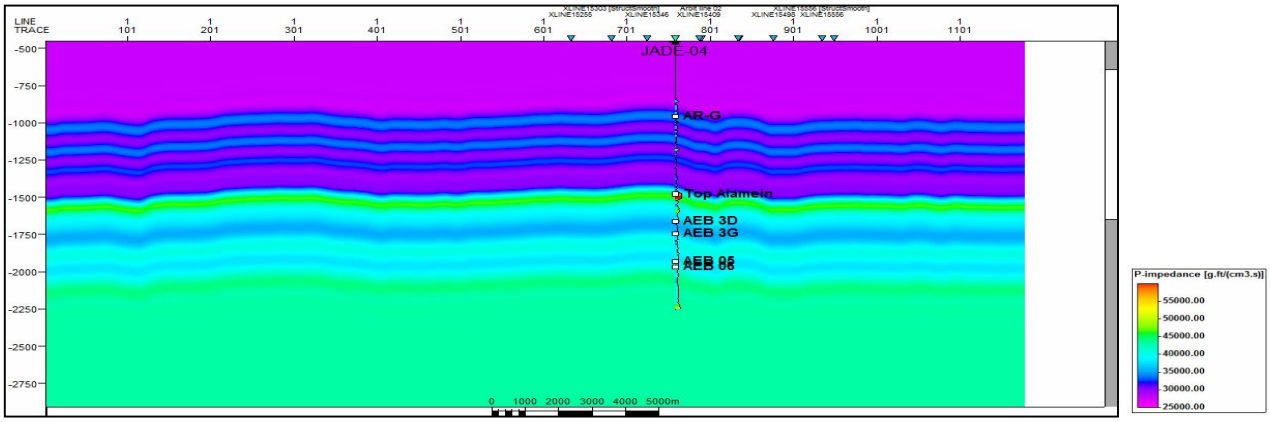

Figure 11: Low Frequency Model for Inline 7817.

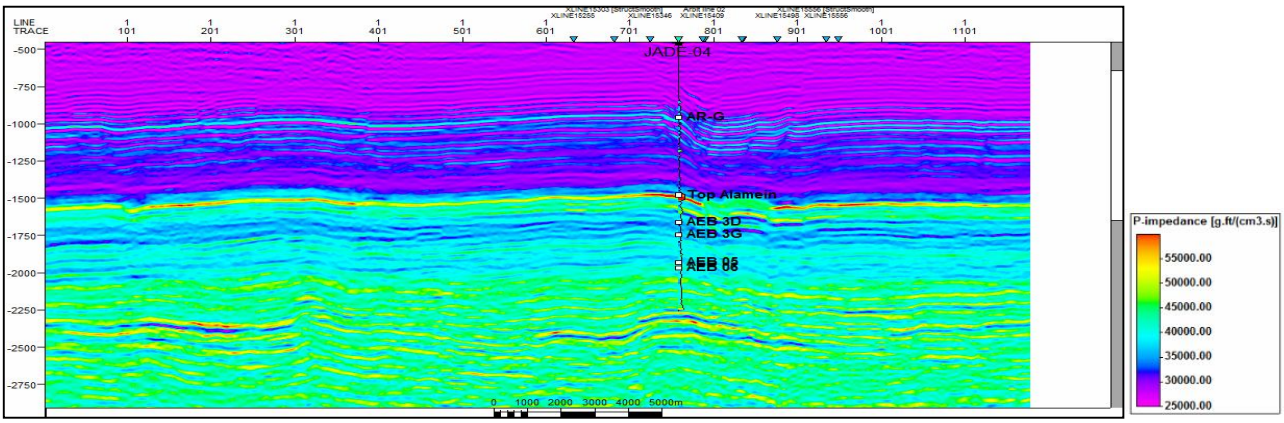

Figure 12: Acoustic Impedance Section for Inline 7817.

CONCLUSION

Post stack seismic inversion approach indicated a patterns can greatly add to conventional direct hydrocarbon interpretation. It has proven to be very useful theory in the detection of the hydrocarbon occurrences and lithological definition in the area of study. Using the results of the experiment by showing the Lower acoustic impedance anomaly has a great impact to confirm the hydrocarbon existence at the zone of interest in our study area which is Alam El Bueib 3G reservoir member. Also, this approach was very helpful by showing of higher acoustic impedance anomaly at the level of Alamein Formation due to the presence of dolomite and shale as seal rocks.

REFERENCES

Buland, A. and Omre, H, 2003, Bayesian linearized AVO inversion, Geophysics, 68, 185-198.

Curia, D., 2009, Seismic inversion methods: Avo Azimutal (Avaz) En La Detección De Fracturas: Caso De Estudio En Tres Campos De Repsol-Ypf Cuenca Neuquina, Argentina. IX Congreso Argentino de Exploracion de Hidrocarburos, 2004

Geophysical Society of Houston (various authors), 1973, Lithology and direct detection of hydrocarbons using geophysical methods

Greenberg, M. L., and J. P. Castagna, 1992, Shear-wave velocity estimation in porous rocks: Theoretical formulation, preliminary verification and applications: Geophysical Prospecting, **40**, 195-210.

Hampson Russell, 2004, STRATA Training Workshop Documentation

Hosny, A. Master Thesis, Ain shams university, Faculty of Science , Geophysics department, Cairo, Egypt "Post and Pre-Stack Seismic Inversion Techniques for Reservoir Characterization, Simian Field, Offshore Nile Delta –Egypt"

Russell, B. and Hampson, D., 1991, A comparison of post-stack seismic inversion methods: Ann. Mtg. Abstracts, Society of Exploration Geophysicists, 876-878.

Simmons, J.L. and Backus, M.M., 1996, Waveform-based AVO inversion and AVO prediction-error, Geophysics, 61, 1575-1588.

Egyptian Geophysical Society
EGS Journal, Vol. 15, No. 1, 97-106 (2017)

GEOTHERMAL PARAMETERS ESTIMATION UTILIZING DIFFERENT TECHNIQUES OF PETROPHYSICAL INTERPRETATION AND WELL LOGGING ANALYSIS AT AL QASR FIELD, WESTERN DESERT, EGYPT

A.S. Helaly[(1)], A.M. Elsayed[(1)] and N.R. Elsaadany[(2)]

(1) Geophysics Department, Faculty of Science, Ain Shams University, Cairo, Egypt.
(2) Petrosannan Co.

التعرف على الخصائص الحرارية للخزان الجوفى علم البويب 3E باستخدام بيانات الآبار فى منطقة القصر بالصحراء الغربية – مصر

الخلاصـــة: تهدف هذه الدراسة الى تقييم مدى الاستدامة الحرارية للخزان الجوفى علم البويب AEB-3E فى حقل بترول القصر بالصحراء الغربية من خلال استخدام البيانات و التسجيلات الكهربية المختلفة لحساب الخصائص البتروفيزيقية و عمل نموذج للتركيب المعدنى للخزان لاستخدام هذا النموذج فى حساب الخصائص الحرارية للخزان للوصول الى مدى امكانية استخدام المياه الحارة المنتجة من الخزان فى عمل وحدة كهرباء بقدرة ٤٥٠ كيلو وات لخدمة اغراض الحقل. وتشمل البيانات المتاحة لهذه الدراسة على بيانات رقمية لتسجيلات الآبار في صورة تسجيلات المقاومة الكهربية العميقة والضحلة والكثافة والمسامية والنيترون إلى الارتداد الصوتي وأشعة جاما والعديد من التسجيلات الرقمية الأخرى . بدأت الدراسة بعرض مختصر للتـــاريخ الجيولـــوجي والتركيبي للمنطقة عبر العصور الجيولوجية المختلفة من خلال إلقاء الضوء على ما تم التوصل إليه من نتائج العديد من الباحثين ثم انتقلت الدراسة إلى عرض تاريخ علم تسجيلات الابار و اجهزة التسجيل المختلفة ثم توضيح خطوات الدراسة التى تتمثل في : -عمل تحليل بتروفيزيقي باستخدام تسجيلات ا بار المتاحة لحساب الخواف البتروفيزيقية مثل: (التشبع البيدروكربوني،التشبع المائي ،النطاقات المنتجة،المسامية الكمية والمسامية المؤثرة) - عمل خرائط للخواص البتروفيزقية المتاحة مثل(:خرائط المسامية،خرائط التشع المائي والهيدروكربونى ، خرائط توزيع محتويات كل من الرمل و الطفلة بتفسير هذه الخثث الخرائط يمكن معرفة الاسباب المؤدية للتغيير الافقي للصفات البتروفيزيقية في منطقة الدارسة. - عمل رسوم بيانية للنتائج المختلفة للخزانات المدروسة مثل : (المقاومة ، الكثافة، المسامية مع علاقات التشبع السائمى والمحتويات الميثولوجية) للتعرف على المكونات الميثولوجية لصخور الخزانات فى منطقة الدارسة وتفسير للأسباب التى تؤدى الى التغيير الراسى للخواص البتروفيزيقية. - عمل نموذج للتركيب المعدنى للخزان و حساب نسبة كل معدن بالنسبة للحجم الكلى. استخدام نموذج و حسابات التركيب المعدنى بالضافة الى الخواص البتروفيزيقية لحساب الخواص الحرارية المختلفة للخزان. - عمل خرائط للخـــواص الحرارية لمعرفة تغير هذه الخصائص فى منطقة الدراسة. -تحديد الاماكن ذو الخواص الحرارية المختلفة. -حساب الطاقة الحرارية الكلية التى يمكن استخراجها من الخزان. واعتمادا على نتائج الخطوات السابقة تم تصميم نموذج لانشاء وحدة كهرباء تستغل المياه الحارة المنتجة من هذه الابارو عمل دراسة جدوى اقتصادية للمشروع.

ABSTRACT: *Estimating the geothermal parameters from the interpretation of well logging data can be applied in case of the paucity of core data for direct measurements .Such approach depend on the construction of mineralogical model for the studied reservoir by using different types of mineralogical plots, then estimating the volume of each individual mineral and the total porosity for the reservoir. To estimate the thermal conductivity, the geometric average of individual conductivities weighed by the volumetric proportion of each mineral, the heat flow, geothermal gradient and radiogenic heat production can be defined. The geothermal properties of AEB-3E reservoir was defined by using the well logging data from 5 wells (Qasr-4, Qasr-40, Qasr-31, Qasr-37 and Qasr-35).The structure is a three way dip closure. Three oil producer wells were drilled on the crest of the trap (Qasr-4, Qasr-31 and Qasr-40), and then two wells were drilled in the down dip direction which were totally water saturated. The analysis of the data shows incraesement of clay content with the down dip direction. Thermal conductivity values increase toward north from 2.8 W/m/K in Qasr-35 and 2.9 W/m/K in Qasr-37 to 3.4 W/m/K in Qasr-40, 3.4 W/m/K in Qasr-31 and 3.6 W/m/K in Qasr-4. Heat flow of AEB-3E reservoir was calculated for each individual well, the results show the same pattern of thermal conductivity, increasing in heat flow from the southern wells with average values 80 mW/m^2 in Qasr-35 and 84 mW/m^2 in Qasr-37 to northern with average values 93 mW/m^2 in Qasr-31 98 mW/m^2 in Qasr-40 and 112 mW/m^2 in Qasr-4, specially toward north – west direction at Qasr-4.*

INTRODUCTION

This study aims to determine the mineralogic model of the studied reservoir AEB-3E in Qasr-4, Qasr-40, Qasr-31, Qasr-37 and Qasr-35 wells and to estimate the geothermal parameters from this model.

The study area is a three way dip closure trap, five wells were drilled, initially three wells Qasr-4, Qasr-40, Qasr-31 were oil producers located at the crest of the structure, two wells Qasr-37 and Qasr-35 were drilled in the down dip direction were totally saturated with water as shown in figure (1). The producer wells (Qasr-4, Qasr-40, Qasr-31, now produce oil with very high water cut. This hot water comes from deep reservoir (AEB-3E) with high temperature due to the normal geothermal gradient, that consider a waste water resources referred to the produced water from oil and gas wells, co- produced geothermal fluids are hot and

are often found in waterflood fields in a number of Western Desert oil and gas production regions.

This water is typically considered a nuisance to the oil and gas industry (and industry is accountable for proper disposal), but could be used to produce electricity for internal use or sale to the grid.

The high volumes of saltwater produced during hydrocarbon production, combined with the high bottom hole temperatures found in the Western Desert at depth, provide an ideal mix of resources from which to produce electricity from geothermal energy.

The development of this resource requires an understanding of both the business model and geologic setup involved.

The existing infrastructure and expertise of the oil and gas industry in this area affords us the opportunity to leverage that investment and combine geothermal energy production with hydrocarbon and waste heat production.

Depending on the available data of the oil or gas wells, this data can be used for generating a picture about the geothermal system and estimating the sustainability of these geothermal fluids as a source of heat; by which electricity can be generated through a new low-temperature electric generation technology (ORC) that can develop the geothermal resources economically today.

AEB-3E reservoir study is an example for estimating the availability to apply is concept on the other suitable fields that have the same conditions.

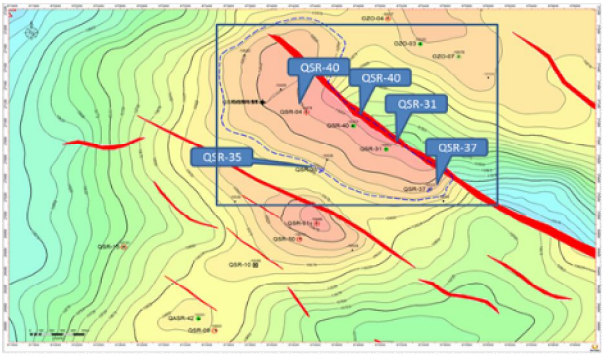

Fig. (1): AEB-3E Structure Map.

The reconstruction of the mineralogic model and fluid content of this reservoir from the available well log data, such as Neutron, Density and Sonic; to estimate the geothermal parameters is the main target of this study. Crossplots assist in the selection of the interpretation parameters and the identification of the trends and problems of mineralogic model. The formerly mentioned crossplots are based on knowing and plotting the matrix coefficient of any mineral, which helps in driving the mineral constituents of the studied rock intervals. The minerals present in this reservoir are identified through different crossplots.

Geological setting of the study area:

The Qasr/Ozoris area is located on a broad terrace that separates Shushan Basin. That lies -15 km to the west, from the Khalda Ridge -15 km to the east a smaller sub-basin. Informally termed the Wanda Sub-basin lies to the north of the Ozoris/Oasr area to the south, the E-W trending Qattara ridge forms the southern limit of this area. The Ozoris/Qasr terrace is dissected by WNW-trending faults, which were initiated during the Cretaceous and continued moving until recent times. These faults overlay a Jurassic system of dominantly NE-SW trending faults, which define structures from the Masajid Limestone to Paleozoic rocks. Minor NW-SE trending Jurassic and older faults are subordinate to the main fault trends. The oldest rocks in the region are believed to be Silurian, from a core of this section in North Ghazaial-I X However, the oldest rocks penetrated in the Qasr area are Early Jurassic. The Jurassic age was a period of NW-SE regional extension, which reactivated Paleozoic structures and caused deepening within the main depocentres such as Shushan Basin during this time, thick fluvial to shallow marine sands of the Lower Safa Fm. were deposited over the southern half of the Khalda Offset area and on the southern part of the Khalda Ridge. As erosion rates coal swamps and fluvial to shallow marine shales and minor sandstones of the Upper Safa Fm were deposited. These carbonaceous sediments that are believed to be the main source rocks in the region. Renewed tectonism in the late Jurassic caused the region east of Shushan Basin to break into a series of tilted fault-blocks. These were then eroded prior to a marine incursion and deposition of the Masajid Fm limestones to the north of the Qasr area. Tectonism was renewed in the Early Cretaceous and erosion of the Masajid Fm witnessed the reworking of limey material deposited as the AEB-6 unit in local depocenters. Later, fluvial to shallow marine sands of the Alam El Bueib Fm were deposited as a transgressive sequence over the area, such as Qasr. This system culminated with the deposition of the Alamein Dolomite and Dahab shales, before repeating-itself with the Kharita, Bahariya and Abu Roash transgressive sequence.

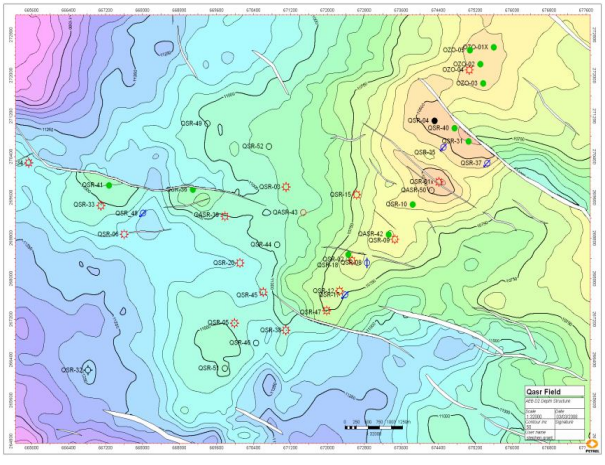

Fig. (2) Qasr Field (AEB-3E) Depth Structure After KPC (2004).

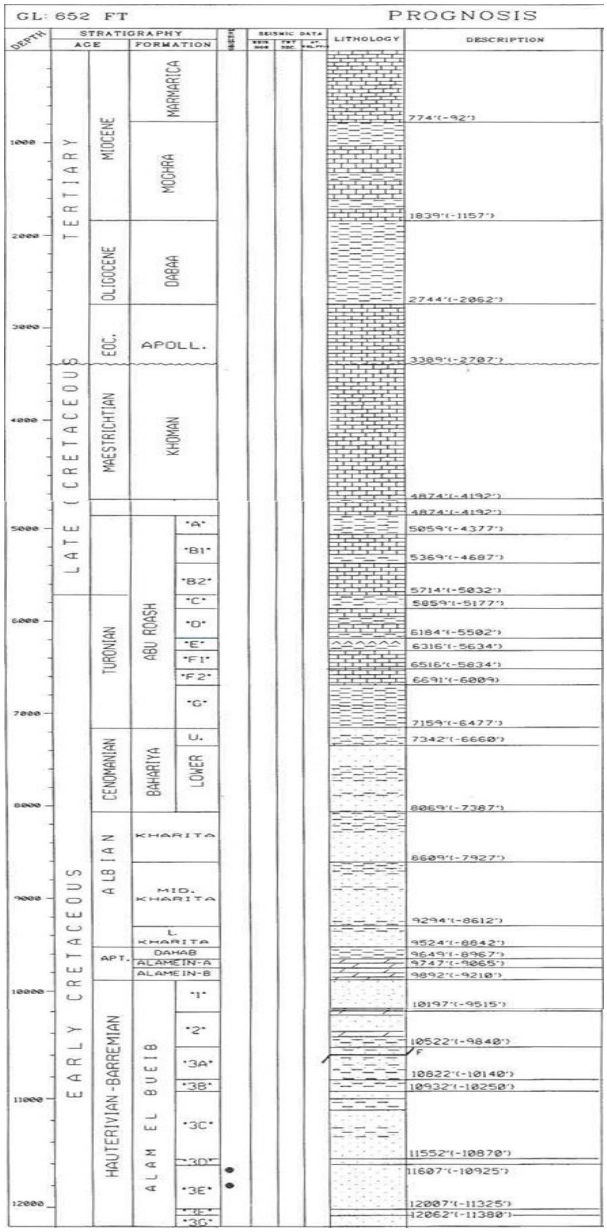

Stratigraphic Column for the study area.

Petrophysical Methodology and Techniques:

Mineral Identification model:

The identification of a bed's lithology is considered a fundamental issue to all reservoir characterization studies because the physical and geothermal properties of the rock that holds hydrocarbons and/or water affect the response of every tool used to measure the formation properties. Understanding the reservoir lithology is the foundation from which all other petrophysical calculations are made. To make accurate petrophysical calculations of porosity, water saturation (S_w), and permeability, the various lithologies of the reservoir interval must be identified and their implications should be understood. Lithology identification model has been estimated from a number of crossplots between the different logging tools to identify the main components of AEB-3E reservoir and the volume of each one.

Neutron- Density Crossplot:

The Neutron- density crossplots are commonly used to determine the lithology (using the neutron and density logs) and accurately evaluate the matrix porosity of carbonate rocks. In this case, the bulk density (ρ_B) and neutron porosity (φ_N) readings are plotted together. For points corresponding to particular water-saturated zone, pure lithologies can be defined by lines (representing quartz, limestone, dolomite) which show gradual change in porosity units; or a single zero-porosity point (e.g., salt point) may be defined. When the matrix lithology is a binary mixture (e.g. quartz – limestone or limestone-dolomite); the points plotted from the log readings will fall between the corresponding lithology lines.

The neutron-density crossplot for AEB-3E reservoir in Qasr-4, Qasr-40, Qasr-31, Qasr-37and Qasr-35 wells reflect that the plotted points are scattered on sandstone and between sandstone and limestone lines with porosity $\Phi_{N\text{-}D}$ ranging from 8% to 17%, 10% to 18%, 7% to 15%, 8% to 17% and 12% to 20% respectively as shown in figures (1,2,3,4,5). Some points are scattered downward through dolomite line due to the effect of shale. This indicates the presence of shaly lithology mixed with sandstone intervals. The change of color points from violet to red show the degree of cleanness.

The effect of hydrocarbon isn't observed in Qasr-4, Qasr-40and Qasr-31wells due to the deep invasion.

Photoelectric - Density crossplot:

The bulk density versus photoelectric cross section index crossplot can be used to determine porosity and to identify the mineral in a single-mineral matrix. Also, the charts can be used to determine porosity and the mineral fractions in a two mineral matrix where the minerals are known.

Photoelectric cross section-density crossplot for AEB-3E reservoir in Qasr-4, Qasr-40, Qasr-31, Qasr-37and Qasr-35 wells; reflect that the plotted points are scattered on sandstone and between sandstone and dolomite lines which means no limestone in the matrix. The porosity ranging from 5% to 17%, 10% to 18%, 5% to 15%, 8% to 16% and 8% to 20% respectively. Some points are scattered downward through dolomite line due to the effect of shale. This indicates the presence of shaly lithology mixed with sandstone streaks as shown in figures (6, 7, 8, 9, 10).

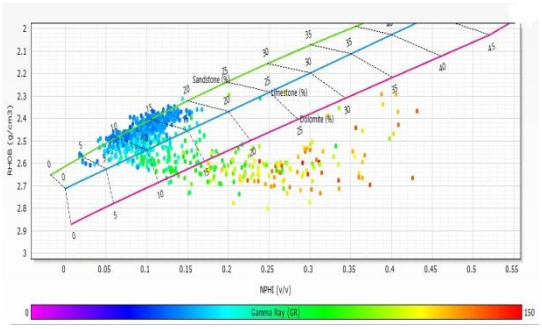

Fig. (1): The Neutron-Density crossplot for AEB-3E reservoir in Qasr-4

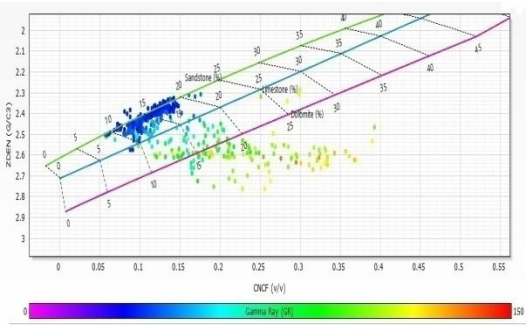

Fig. (2): The Neutron-Density crossplot for AEB-3E reservoir in Qasr-40

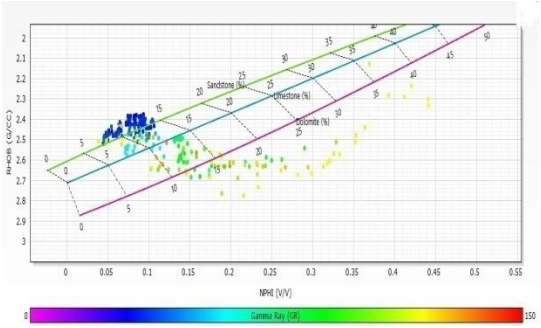

Fig. (3): The Neutron-Density crossplot for AEB-3E reservoir in Qasr-31

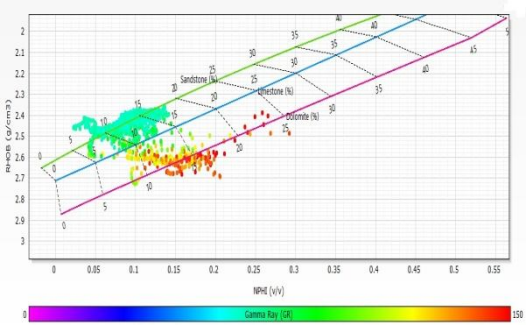

Fig. (4): The Neutron-Density crossplot for AEB-3E reservoir in Qasr-37

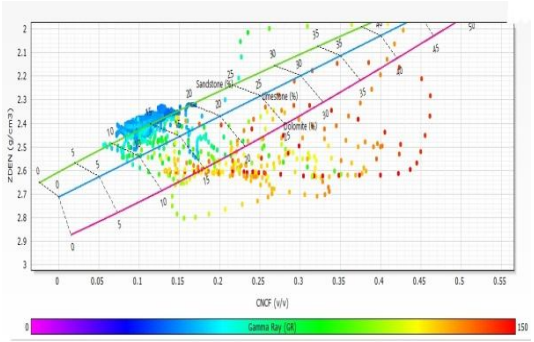

Fig. (5): The Neutron-Density crossplot for AEB-3E reservoir in Qasr-35

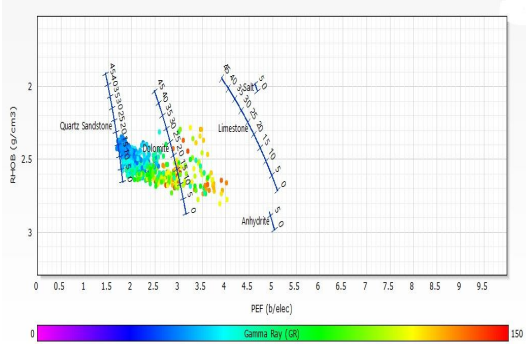

Fig. (6): Photoelectric - Density crossplot for AEB-3E reservoir in Qasr-4

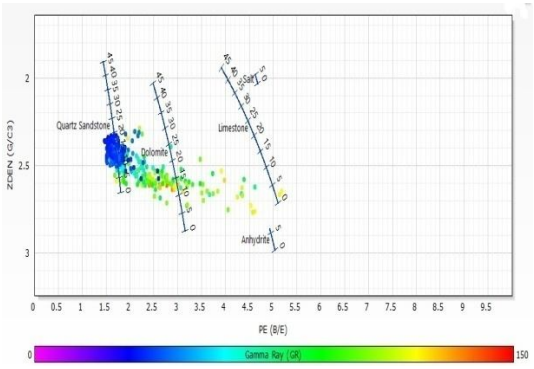

Fig. (7): Photoelectric - Density crossplot for AEB-3E reservoir in Qasr-40

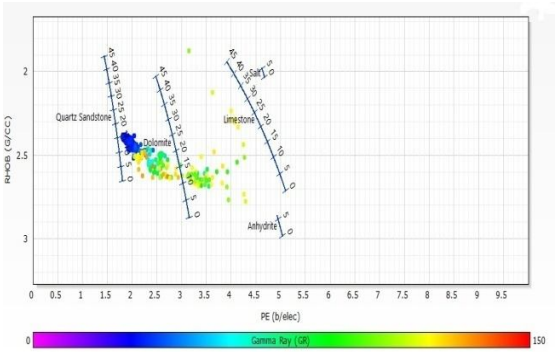

Fig. (8): Photoelectric - Density crossplot for AEB-3E reservoir in Qasr-31

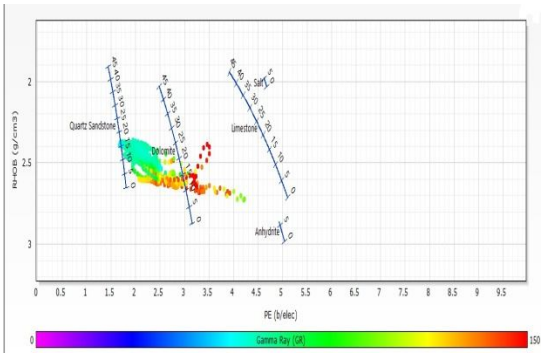

Fig. (9): Photoelectric - Density crossplot for AEB-3E reservoir in Qasr-37.

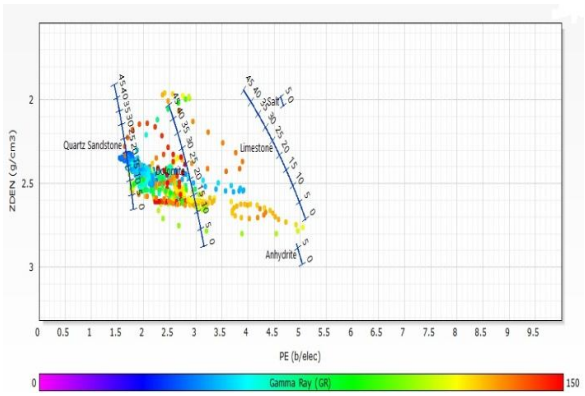

Fig. (10): Photoelectric - Density crossplot for AEB-3E reservoir in Qasr-35.

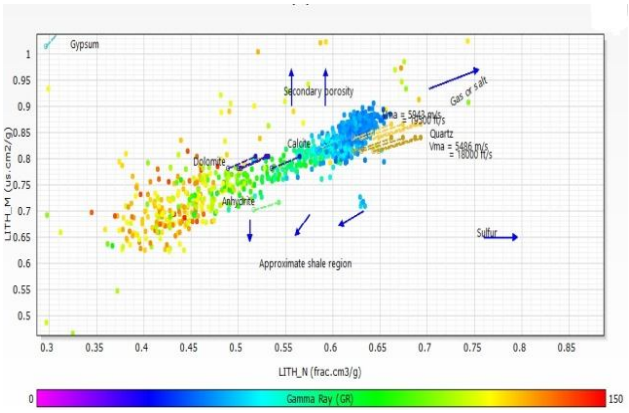

Fig. (11): M-N Crossplot for AEB-3E reservoir in Qasr-4.

M- N Crossplot

Lithology interpretation with neutron, density, and sonic logs is facilitated through the use of M-N plots. This plot was first introduced by (Bruke et al., 1969**)**. It combines the data of all three porosity logs to provide the lithology-dependent quantities, M and N, which are essentially independent of primary porosity.

M-N Crossplot for AEB-3E reservoir in Qasr-4 reflect that the plotted points are scattered between sandstone and limestone lines, and some points are scattered downward through dolomite line due to the effect of shale. This indicates the presence of shaly lithology mixed with sandstone streaks as shown in figure (11).

MID Lithology Plot:

The MID (Matrix Identification) plot, is considered as complementary approach for identifying the lithology, gas and secondary porosity. It depends on the apparent matrix density (ρ_{ma}) and apparent transit time (Δt_{ma}) for clean and shaly zones. They are used in the MID plot to define the association of essential and accessory minerals that form the background of matrix in the analyzed rocks of the considered zones.

MID Lithology Plot for AEB-3E reservoir in Qasr-4 reflects that the plotted points are scattered between sandstone and limestone points, while, some points are scattered downward through dolomite point due to the effect of shale. This indicates the presence of shaly lithology mixed with sandstone streaks. Some points scattered toward gas direction due to the gas effect as shown in figure (12).

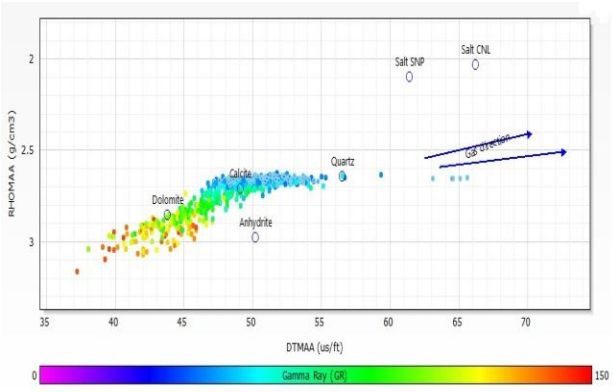

Fig. (12): MID Lithology Plot for AEB-3E reservoir in Qasr-4.

Litho-saturation Crossplots:

The litho-saturation crossplots for all available wells were constructed to show the vertical distribution of the minerals occurrences within the studied reservoir.

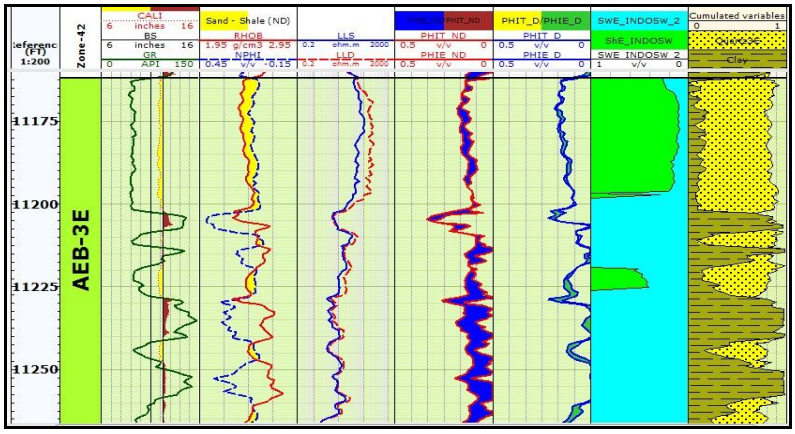

Fig. (13): The litho-saturation crossplot of AEB-3E member in Qasr-4.

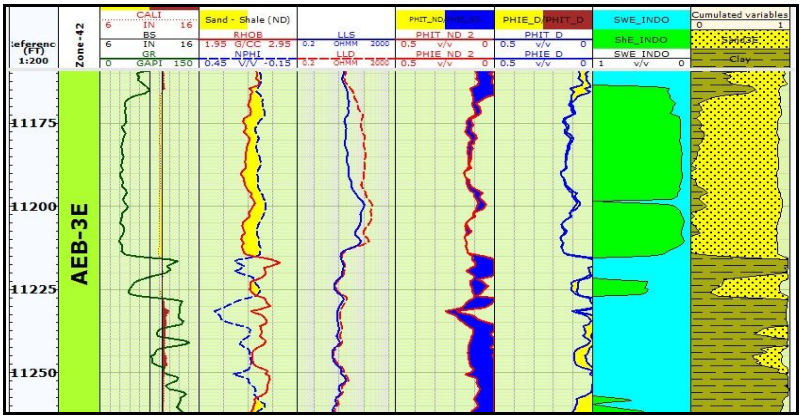

Fig. (14): The litho-saturation crossplot of AEB-3E member in Qasr-31.

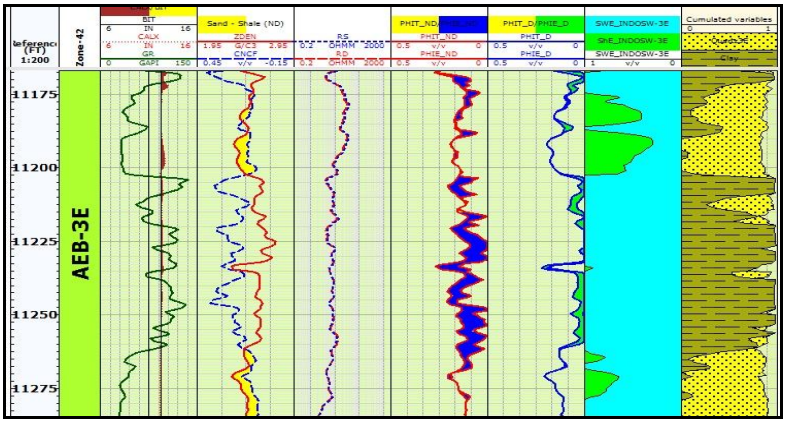

Fig. (15): The litho-saturation crossplot of AEB-3E member in Qasr-40.

These plots illustrate a number of continuous curves relating the calculated variables in the rock materials and petrophysical parameters with depth such as rock porosity, and saturation matrix content.

The litho-saturation crossplot of AEB-3E reservoir in Qasr-4,Qasr-40,Qasr-31,Qasr-37 and Qasr-35 wells indicates intercalations of sandstone with an average clay content of about 20%, 20%,23%, 29%,30% respectively, as shown in figures (13, 14, 15, 16, 17).

The litho-saturation crossplot of AEB-3E reservoir in Qasr-4 and Qasr-31 figures (13, 14) shows clean sandstone intervals saturated with hydrocarbon intercalated with some clay streaks in-between , where the average clay content in the clean intervals are about 13% and 12% respectively. The high resistivity of the clean intervals shows a good separation between the three different types of resistivity that refers to deep invasion through the reservoir. This indicates good permeability and mobility. The average hydrocarbon saturation within the reservoir intervals are about 20% and 10% respectively.

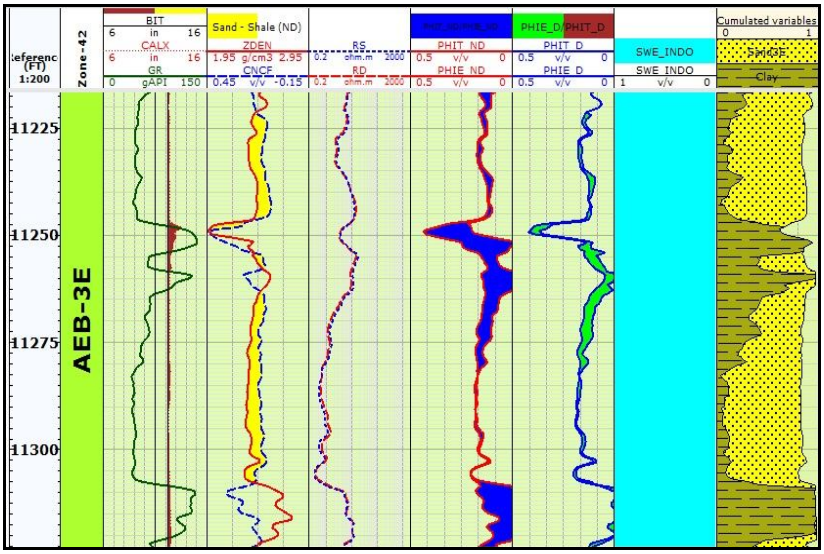

Fig. (16): The litho-saturation crossplot of AEB-3E member in Qasr-37.

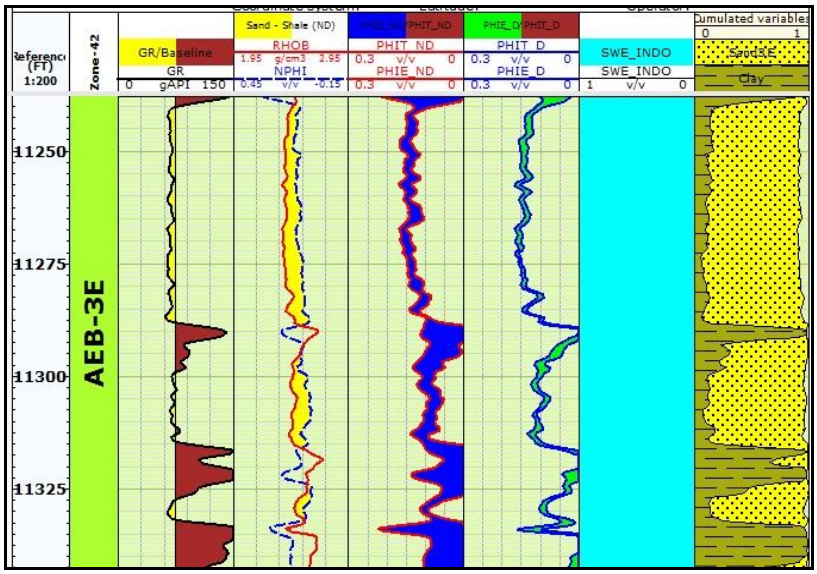

Fig. (17): The litho-saturation crossplot of AEB-3E member in Qasr-35.

Table (1): The petrophysical parameters of AEB-3E reservoir.

Name	Depth to Top TVDSS (ft)	Depth to Bottom TVDSS (ft)	Thickness (ft)	Average ϕ_{eff} %	Average ϕ_t %	average sw %	V_{sand} %	V_{clay} %
Qasr-4	10478.8	10888.2	409.4	12	15	20	63	20
Qasr-40	10487.9	10714.3	226.4	15	17	38	63	20
Qasr-31	10489.3	10604.7	115.4	15	15	14	61	23
Qasr-37	10608.8	10868.0	259.2	11	18	100	54	29
Qasr-35	10557.0	10790.5	233.5	11.1	16	100	53	30

The litho-saturation crossplot of AEB-3E member in Qasr-40 shows the same sandstone properties as Qasr-4 and Qasr-31 with higher water saturation value due to lower resistivity, the average saturation is about 35% as shown in figure (15).

Qasr-37 and Qasr-35 are structurally lower than the three other wells, the litho-saturation crossplot shows sandstone intervals totally saturated with water and with higher clay content than the other wells with an average amount of about 30% as shown in figure (16, 17).

Based on the previous model, the weighted averages for the petrophysical parameters of AEB 3E reservoir were calculated in the studied wells, as summarized in table (1) .

Gothermal Methodology and Techniques:

Thermal Conductivity :

Thermal conductivity is dependent on the composition and geometry of the rock matrix, porosity, and medium-pore water or hydrocarbons. Additional influences in the situation of a deeply buried rock; are pressure and temperature.

Measurements of thermal conductivity cover a wide spectrum of techniques, that can be subdivided into direct (laboratory) and indirect (well logging) approaches. Some studies focused on determining the thermal conductivity from well logs. Based on the detailed lithologic description together with the sonic and neutron logs, they were digitized and used for estimating the thermal conductivity.

In this study, the in-situ thermal conductivity is based on the volumetric distribution of the mineral constituents, total porosity and fluid content of the studied rock units obtained from well log data and, then the geometric mean method was used for estimating thermal conductivity of the zone of interest.

Geometric Mean Method for Estimating Thermal Conductivity:

The wide variety of thermal conductivity values for the rock-forming minerals found in Table (2) and the results obtained in this study revealed that: the knowledge of the complete mineralogy of the rock as shown in mineral identification model is necessary for the accurate assessment of the rock's thermal conductivity. Based on the mineralogical composition, the values of corrected thermal conductivity "***Ƙ***" in (W/m/k) for the different zones in the studied rock units can be computed from the generalized geometric mean method, as expressed by equation (1), a method that was successfully used by Woodside and Messmer, (1991) and Sass et al., (1971):

$$Ƙ_m = \prod_{i=1}^{n} Ƙ_i^{v_i} \quad \text{.....(1)}$$

where: π represents the product of the thermal conductivities of the minerals "***Ƙ***" raised to the power of their volumetric proportion **v**, in which the sum of the volumetric proportions of the minerals is equal to 1. The subscript ***i*** refers to the mineral, there being **"n"** minerals altogether. Equation (2) gives the best results when the thermal conductivity of each mineral does not contrast by more than one order of magnitude. Thermal conductivity "**Ƙ**" of a porous medium can be expressed as:

$$Ƙ = Ƙ_s^{(1-\Phi)} Ƙ_w^{\Phi} \quad \text{.....(2)}$$

Where: **"Ƙ"** is the in-situ thermal conductivities, **Φ** is the total porosity, "$Ƙ_s$" is the conductivity of the solid matrix, and "$Ƙ_w$" is the conductivity of the pore-filling fluid, in this case water.

In this discussion of the thermal conductivity, it has been assumed that, the conductivity is isotropic. Table (2) shows the measured thermal conductivity of different minerals as follows.

Table (2): Thermal conductivity values for different matrices, after F. Maky and A.M. Ramadan 2010

Matrix	Thermal conductivity W/m/k
Quartz	7.8
Calcite	3.4
Dolomite	5.1
Anhydrite	6.4
shale	2.8
Silt	1.65
Water	0.6
Oil	.21
Gas	.079

Geothermal Gradient Determination:

The corrected "BHT's" are used to estimate an average temperature gradient for the wells. The equilibrium gradient is calculated as equation (3):

$$\frac{dt}{dz} = \frac{BHT - TS}{Z} \quad \text{.....(3)}$$

Where "**BHT**" is the corrected temperature, **"TS"** is the average surface temperature, both in °C, and "**Z**" is the true vertical depth of the log measurement in feet.

Heat Flow Determination

Heat flow "q_0" was estimated using the interval method. It is given by the Fourier`s law of heat conduction, as equation (4):

$$q_0 = K\frac{dt}{dz} \ldots\ldots\ldots\ldots (4)$$

Where: "q_0" is the surface heat flow, "K" is the average of the corrected thermal conductivity of the interval and "**dt/dz**" is the geothermal gradient.

Radiogenic Heat Production:

Rocks produce a natural radioactivity due to the decay of natural radioactive elements. The three types of isotope decay series abundant in the different types of rocks are the Uranium series (decay of ^{238}U and ^{235}U), the thorium series (decay of ^{232}Th), and the decay of potassium isotope ^{40}K, which is much more abundant in the shaly rocks.

In this study, the radiogenic heat production is based on the relation developed by **Bücker and Rybach**, that uses a linear relationship between the natural total gamma-ray logs from industrial oil exploration (in API units) and the laboratory measured heat production "A" in $\mu W/m^3$, as shown in equation (5)

A = 0.0158 (GR [API] – 0.8 …….(5)

Where: A: Radiogenic Heat in $\mu W/m^3$.

GR: Gamma Ray value in (API) from electric log.

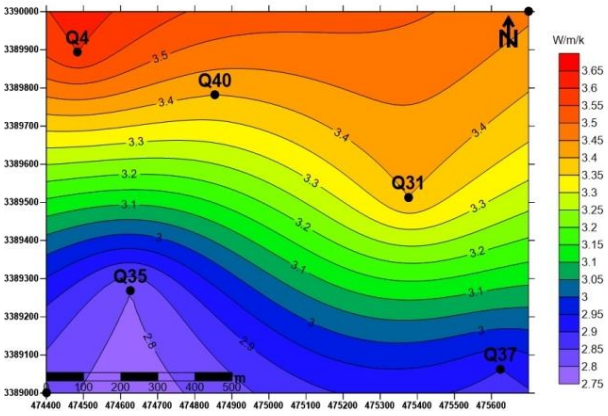

Fig. (18): Thermal conductivity map for AEB-3E Reservoir.

RESULTS

Geothermal Properties of AEB-3E Member:

Based on the results of mineral identification model, AEB-3E member consists mainly of sandstone beds intercalated with clay streaks. The presence of quartz matrix in this member increases its thermal conductivity due to the high value of its matrix thermal conductivity as shown in table (2), which affects the other geothermal parameters as well. For the study area, the thermal conductivity values increase toward north from 2.8 W/m/K in Qasr-35 and 2.9 W/m/K in Qasr-37 (south) to 3.4 W/m/K in Qasr-40 , 3.4 W/m/K in Qasr-31 and 3.6 W/m/K in Qasr-4 (towards north) as shown in figure (18). The increase of thermal conductivity is due to the increase of sand volume which increases toward north from 53% in Qasr-35 and 54% in Qasr-37 to 61% in Qasr 40, 61% Qasr 31 and 63% in Qasr-4 as shown in figure (19)

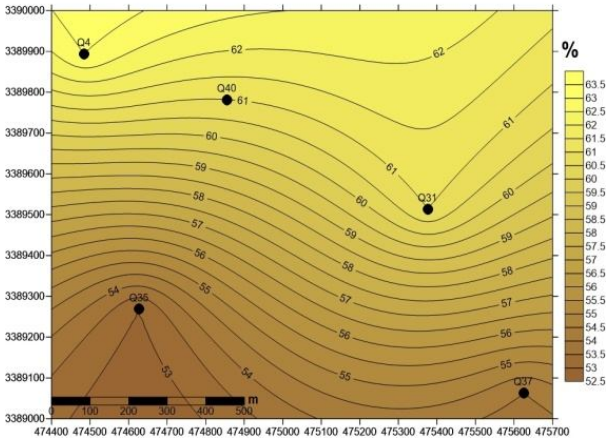

Fig. (19): Net sand map for AEB-3E Reservoir.

After estimating the geothermal gradient using equation (3), it was found it has an average of **30 °C/km.** The average heat flow of AEB-3E member was calculated using equation (4) for each individual well. The results show the same pattern of thermal conductivity, increasing in heat flow from the southern wells with average values of 80 mW/m^2 in Qasr-35 and 84 mW/m^2 in Qasr-37 to north with average values 93 mW/m^2 in Qasr-31 98 mW/m^2 in Qasr-40 and 112 mW/m^2 in Qasr-4, specially toward northwest direction at Qasr-4 well as shown in Figure (20).

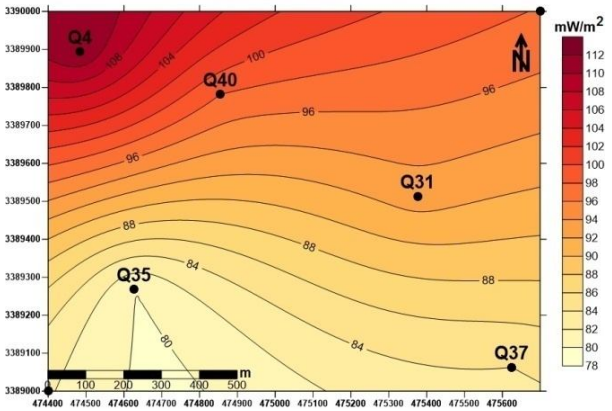

Fig. (20): Heat flow map for AEB-3E Reservoir.

Radiogenic heat production was estimated from GR log using equation (5). The heat production at each well depends on the GR values and the clay content. The estimated values were mapped, and showing a decreasing in heat production toward north with decreasing of clay content (figure 21), which matches with the other geothermal properties of the reservoir.

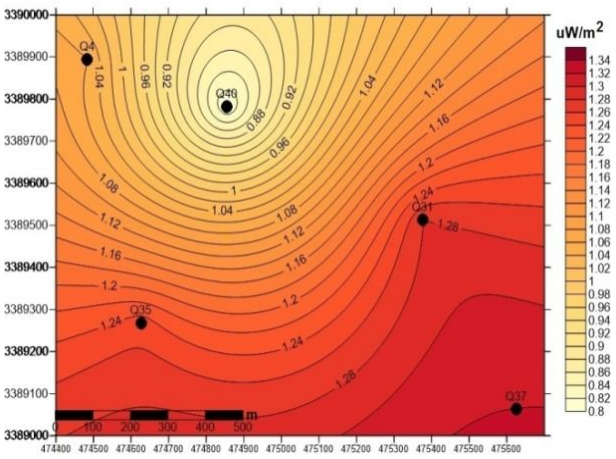

Fig. (21): Heat Production map for AEB-3E reservoir.

CONCLUSION

The mineralogical composition and their volumetric distribution of the analyzed reservoir studied in the area around five wells is determined from the recorded well log data and various types of cross-plots. This model shows that, most of the reservoir is mainly composed of quartz with intercalated clay streaks. This reservoir is characterized by gradual increase of thermal conductivities from the south at wells (Qasr-37 and Qasr-35) to the northern part of the study area at wells (Qasr-4, Qasr-40 and Qasr-31) due to the decrease of the clay content toward north direction. Heat flow values show gradual increase toward north compatible with the thermal conductivity values and the decrease of clay content. Radiogenic heat production gradually decreases from south in (Qasr-37 and Qasr-35) with the higher clay content toward north in wells (Qasr-4, Qasr-40 and Qasr-31) with the lower clay content.

Generally, thermal conductivity, heat flow and the radiogenic heat production in the reservoir is highly affected by the lithologic composition, which is characterized by the decrease of clay content toward south, lead to decrease in thermal conductivity and heat flow, and high radiogenic heat production. Therefore, the loss in heat production is low, which leads to the preservation of heat energy. The northern wells are characterized by the increase of sands of higher thermal conductivity and higher heat flow, so the heat is transferred easily to the pore fluids. So the recorded bottom-hole temperature in the southern wells (Qasr-37 and Qasr-35) is lower than the recorded bottom hole temperature in the northern wells (Qasr-4, Qasr-40 and Qasr-31).

REFERENCES

Bigelow, L., (1995): Introduction to Wireline Log Analysis, Western Atlas International, Inc., Houston, Texas-USA.

Bruke, J.A.; Campbell, R.L.; and Schmidt, A.W., (1969): The litho-porosity crossplot. The log analyst (SPWLA) Vol.10, No.6. p. 25-43

Maky, F.; Abubakr and Ramadan, A.M.; Mohamed 2010: Thermal Conductivity, Radiogenic Heat Production and Heat Flow of Some Upper Cretaceous Rock Units, North Western Desert, Egypt, Journal of Applied Sciences Research, 6(5): 483-510, 2010

Poupon, A. and Leveaux, J. (1971): Evaluation of Water Saturations in Shaly Formations. The Log Analyst 12 (4).

Pribnow, D. and J.H. Sass, 1995. Determination of thermal conductivity from deep boreholes: Journal of Geophysical Research, 100: 9981–9994.

Sass, J.H., A.H. Lachenbruch and R.J. Muntor,1971 . Thermal conductivity from rock measurements on fragments and its application to heat flow determinations, Jour. of Geophy. Research, 79: 3391-3401.

Schlumberger, (1972): ''Log interpretation'' volume I, principle, Paris, France

Schlumberger, (1972): The essential of log interpretation practice'' Paris, France

Woodside, W. and J. Messmer, 1961a. Thermal conductivity of porous media: I. Unconsolidated sands: Journal of Applied Physics, 32: 1688–1699.

Woodside, W. and J. Messmer, 1961b. Thermal conductivity of porous media: II. Consolidated sands: Journal of Applied Physics, 32: 1699–1706.